GROUND-MOTION SCALING IN THE WESTERN ALPS

Paola Morasca [(1)], Luca Malagnini [(2)], Aybige Akinci [(2)],
Daniele Spallarossa [(3)], R. B. Herrmann [(4)]

(1) DIPTERIS, Universita' di Genova, Viale Benedetto XV, 5, 16132 Genova, Italy.
(2) INGV, Viale di Vigna Murata 605, 00143 Roma, Italy
(3) INGV-GNDT, c/o Universita' di Genova, Viale Benedetto XV, 5, 16132 Genova, Italy.
(4) Dept. of Earth and Atmo. Scie. of Saint Louis University

Key words: Attenuation, Ground Motion, Western Alps

Journal of Seismology (submitted)
September, 2004

Abstract

In order to empirically obtain the scaling relationships for the high-frequency ground motion in the Western Alps (NW Italy), regressions are carried out on more than 7500 seismograms from 957 regional earthquakes. The waveforms were selected from the database of 6 three-component stations of the RSNI (Regional Seismic network of Northwestern Italy). The events, M_L ranging between 0.5 and 5.1, were recorded within a hypocentral distance of 200 km during the time period: 1996-2001. The peak ground velocities are measured in selected narrow-frequency bands, between 0.5 and 14 Hz. Results are presented in terms of a regional attenuation function for the vertical ground motion, a set of vertical excitation terms at the reference station STV2 (hard-rock), and a set of site terms (vertical and horizontal), all relative to the vertical component of station STV2.

The regional propagation of the ground motion is modeled after quantifying the expected duration of the seismic motion as a function of frequency and hypocentral distance. A simple functional form is used to take into account both the geometrical and the anelastic attenuation: a multi-variable grid search yielded a quality factor $Q(f) = 310\ f^{0.20}$, together with a quadri-linear geometrical spreading at low frequency. A simpler, bi-linear geometrical spreading seems to be more appropriate at higher frequencies (f>1.0 Hz). Excitation terms are matched by using a Brune spectral model with variable, magnitude-dependent stress drop: at M_w 4.8, we used $\Delta\sigma$=50 MPa. A regional distance-independent attenuation parameter is obtained (κ_0 =0.012 sec) by modelling the average spectral decay at high frequency of small earthquakes.

In order to predict the absolute levels of ground shaking in the region, the excitation/attenuation model is used through the Random Vibration Theory (RVT) with a stochastic point-source model. The expected peak-ground accelerations (PGA) are compared with the ones derived by Ambraseys et al. (1996) for the Mediterranean region and by Sabetta and Pugliese (1996) for the Italian territory.

Introduction

The standard approaches used in hazard assessment generally require transferring the shaking from the earthquake source to the investigated sites. Therefore, understanding the regional wave propagation is crucial for predicting earthquake-induced ground motions. For this reason, the determination of quality factor Q, source parameters and site amplification is an important goal of seismic analysis in seismology.

The anelastic attenuation parameter $Q(f)$ indicates important characteristics of the crustal rocks: large values for the crustal parameter $Q(f)$ indicate quite stable regions, with a lesser amount of circulating fluids and a lesser regional heat flow. Low $Q(f)$ values, on the contrary, characterize active areas of the world (e.g., the Apennines), where large heat flows are measured, and substantial amounts of fluids and volatiles percolate through the crust. The signature of the vertical structure of each specific region of the Earth's crust is mostly inside the geometrical spreading function used to reproduce the observed attenuation. Short-distance geometrical spreading always deal with body-waves, and consequently with spherical propagation. Large distances, on the contrary, are related to cylindrical propagation (surface-waves). Both the geometric and the anelastic attenuation may be strongly frequency dependent, since different wavelengths "see" different crustal structures. Moreover, the amplitude and the frequency-dependence of the anelastic attenuation term $Q(f) = Q_0(f / f_{ref})^{\eta}$ may reflect the distribution of the scatters within the crust, and/or the density and saturation of cracks at the specific wavelength (O'Connell and Budianski, 1974).

Recently, many studies show that the ground motion levels are also quite different in zones of different tectonic regimes such as extensional and compressional (Boore et al., 1997, Campell, 1997, Sadigh, et al., 1997, Atkinson and Silva, 1997, Atkinson and Boore, 1995). Moreover, comparing the crustal propagation term of the western Alps with that of other regions, may give us a better understanding of different tectonics and geologic environments (e.g., Switzerland, Bay et al., 2003; Greece, Pino et al., 2001; Turkey, Akinci et al., 2001; Central Europe, Malagnini et al.

2000b; Southern California, Raoof et al., 1999; Northwestern US, Herrmann and Dutt, 1999; Southern Great Basin, Yazd, 1993; Utah and Yellowstone, Jeon and Herrmann, 2004; Mexico, Ortega et al., 2003; Bhuj, India, Bodin et al., 2004).

About Italy, more ground motion studies have already been performed in different regions: the Eastern Alps (Malagnini et al., 2002), the Apennines (Malagnini et al., 2000a; Malagnini and Herrmann, 2000), Sicily (Scognamiglio et al. 2004), and Northern Apennines (Morasca et al. 2004). These studies clearly showed the differences in the basic parameters (i.e., attenuation, source and site-related parameters) in each zone, and their influence in the seismic hazard analysis.

From the engineering point of view, these parameters are also applied to construction of buildings through the building code, and more recently, to the renovation of existing codes. Too often this processes start in the aftermath of destructive earthquakes. An example is given by the event occurred on October 31, 2002, that struck the town of San Giuliano di Puglia (southern Italy), causing the collapse of an elementary school and the death of many children. After this tragic event, a great effort has been undertaken for reevaluating the seismic hazard at the national scale in Italy. A working group has been created at the end of 2003 (mostly researchers from the *Istituto Nazionale di Geofisica e Vulcanologia* – INGV), and a fierce discussion has started on the opportunity of using the regionalized predictive relationships for the ground motion that were already available for part of the Italian territory: one for the Apennines (Malagnini et al., 2000a, Malagnini and Herrmann, 2000), and the second one for the eastern Alps (Malagnini et al., 2002).

For Northwestern Italy, however, we provide regional predictive relationships for the ground motion by using large data sets from the background seismicity, relative to events occurred between 1996 and 2001, and characterized by local magnitudes ranging between about 0.5 and 5.1.

By inverting these large amounts of data, we obtain empirical source, propagation and site terms. In order to obtain a predictive relationship of engineering interest (in terms of peak acceleration, spectral acceleration etc.), the empirical terms are modeled using the stochastic tool called Random Vibration Theory (see Cartwright and Longuet-Higgins, 1956). The major issue related to the use of

weak-motion-based predictive relationships in hazard analysis is that they would be used for predicting the ground motion at large magnitudes, possibly outside the magnitude range of the available regional data set. Although a strong debate went on in the last few years on this topic, we feel that no general answers to this question can be given, and that each case needs to be individually evaluated. In the eastern Alps, for example, the ground motion data set analyzed by Malagnini et al. (2002) was integrated with all the available strong-motion accelerograms recorded during the 1976-1977 seismic sequence. The study by Malagnini et al. (2002) demonstrated the validity of the predictive results of the regional scaling relationships up to a moment magnitude M_w 6.5, the largest magnitude ever recorded in the region.

The predictive relationships described in this study are calibrated using independent estimates of moment magnitude obtained by Morasca et al. (2004) through the waveform modeling of some of the largest earthquakes in the data set.

Tectonic and Geologic Setting

Different kinematic styles exist in Italy, as a result of the complex geodynamic processes that have conditioned the build-up of the Alpine and Apennine chains. The continent-continent convergence between the African and the Eurasian plates during the Alpine orogeny has been responsible for the formation of the Alps, that are mainly characterized by compressional and transpressional structures (e.g. CNR-PFG, 1987; Castaldini and Panizza, 1991; Galadini et al., 2001, Dewey et al., 1973; Polino et al., 1990). The Alps are composed of two folded chains, with opposite orogenic polarity, separated by the Insubric lineament, a major E-W-trending tectonic element. The North-alpine chains are built by a pile of nappes in a sandwich-like structure, where the intermediate oceanic units are enclosed between the underlying European units and overlying African units (Dal Piaz, 1995). Large and thick portions of the crystalline basement of both continental margins are involved in the structures, such as the Helvetic massifs in the Western Alps and lower Austroalpine nappes in

the Eastern Alps. The structure of the Southern Alps is a south-verging thrust belt involving the Permian to Tertiary cover and, partly, the underlying Hercynian crystalline basement (Castellarin, 2001).

Results derived by seismic tomography in the study region (Paul et al. 2001, Kissling, 1993, Kissling and Spakman 1996) suggest that the Western Alps display strong lateral variations both at shallow and deeper levels determining significant effects on the propagation of seismic wavefields. The Ivrea body is an important feature of the region, and represents a high-velocity anomaly (Kissling, 1993, Di Stefano et al. 1999) interpreted as a mantle slice whose effect masks deeper structures (Paul et al. 2001) and creates difficulties for the waveform modeling. At a regional scale, a high-velocity anomaly beneath the Po plain and the northern Apennines has been interpreted as subducting European slab (Kissling and Spakman 1996).

As a consequence of the structural complexity of the Western Alps, it is very difficult to precisely define the depth of the Moho beneath the region (Cattaneo et a. 1999, Kissling, 1993, Kissling and Spakman, 1996). The thickness of the crust seems to be affected by strong lateral variations, and ranges from about 10 km in the Ligurian Sea to nearly 50 km beneath the Alps (Buness et al. 1990). A bathymetric map of the Moho, proposed by Kissling (1993) for the Western Alps, does not give us a complete 3D model, although it evidences the asymmetry of the crustal roots of the region, and suggests a separation of the crust-mantle boundary into three surfaces: the European, the Adriatic and the Apenninic Moho.

The seismic activity of the region is generally moderate (Cattaneo et al., 1999, Eva and Solarino, 1998, Sue et al. 1999), with most of the events within the first 20 km in depth, even though Cattaneo et al. (1999) evidenced the presence of earthquakes characterized by large focal depths. The 23 February, 1887, magnitude 6.3 earthquake was the greatest seismic event in the area in the last thousand years (Ferrari, 1991).

Description of the data set

The area is monitored by the RSNI (Regional Seismic network of Northwestern Italy), managed by the Seismological Group of DipTeRis-GS (Dipartimento per lo studio del Territorio e delle sue Risorse, Sezione Geofisica). At present, the network consists of 29 stations, partially located in the Western Alps and partially in the Northern Apennines (Lunigiana-Garfagnana region): 12 of them are one-component short-period stations, connected via telephone analog telemetry (not used in this study). The other 17 stations are equipped with digital three-component seismometers (Guralp CMG40 and Lennartz LE3D-5s), characterized by a 126-dB dynamic range. Particularly, the Lennartz LE3D-5s has a flat frequency response in a range from 0.2 to 40 Hz and the CMG40 has a flat velocity response in a range from 0.033 to 50 Hz. The acquisition procedure is performed by a dial-up LennartzMars88 MC system provided with a 20 bit A/D converter (ADSP).

We selected more than 7500 recordings from 957 regional earthquakes recorded in the western Alps by the six three-component digital stations located in the region (the other three-component stations are located in the Northern Apennines), during a time period of 1996 – 2001 (see figure 1 and table 1). Although the data set includes seismograms from earthquakes of larger magnitude, up to M_L = 5.1, the bulk of the data set is made from events of magnitude $M_L \leq 2$ (figure 2A and 2B). Local magnitudes were computed using a local magnitude scale calibrated for Northwestern Italy by Spallarossa et al. (2002).

The distribution of the focal depths (figure 2D) shows that the data set consists mainly of shallow events, with only a few ones deeper than 15 km. Figure 3 shows three cross sections that will help understanding the spatial distribution of the events in the data set. The AA′ and CC′ cross sections in figure 3 approximately follow the geometrical structure of the Briançonnais and the Piedmont arc that are characterized by focal depths between 0 and 20 km, respectively. The BB′ cross section clearly shows an increase of the focal depths from west to east, involving deep structures. The

apparent increase of focal depths between 200 and 220 km on the BB' cross section is probably an artifact of the location procedure.

Figure 4 shows the distribution of hypocentral distances of all the available seismograms. The spatial sampling of our recordings is fairly homogeneous, up to hypocentral distances of about 160 km, although there is a larger concentration of events around 50 km (figure 2C). The distance range covered by each station is generally fairly wide, since about 650 events of the data set were recorded at all stations. Finally, figure 5 presents the signal-to-noise (S/N) ratios for our data set calculated in the frequency band between 2.0 and 11.0 Hz, using a time window of 2 seconds.

Station Code	Latitude	Longitude	H (m)	Sensor	Acquisition system	Notes
GENL	44N24.34	08E58.18	80	Guralp CMG40	Lennartz Mars88 MC	since 1995
MONE	44N04.77	07E45.30	1320	Guralp CMG40	Lennartz Mars88 MC	since 1991
NEGI	43N50.86	07E42.23	640	Guralp CMG40	Lennartz Mars88 MC	since 03/1996
TRAV	45N30.76	07E44.82	990	Guralp CMG40	Lennartz Mars88 MC	since 1996
STV2	44N14.73	07E19.56	930	Guralp CMG40	Lennartz Mars88 MC	since 1996
RONL	44N52.88	07E35.89	300	Lennartz LE3D-5s	Lennartz Mars88 MC	since 01/1999

Table 1: three-component stations used in this study

Method and Data Analysis

In this section, we will briefly review the procedure used for the data processing. For a more detailed description of the method, we refer the reader to the papers by Malagnini et al. (2000b, 2002).

The original waveforms, corrected for the instrument response, were bandpass-filtered around a set of 14 sampling frequencies between 0.5 and 14 Hz. Each filter, chosen the central frequency f_c, was obtained by using an 8-pole highpass Butterworth filter with corner frequency at $1/\sqrt{2}$ f_c, followed by an 8-pole lowpass Butterworth filter with corner at $\sqrt{2}$ f_c. (see Malagnini et al., 2000b). The peak value of each filtered time history is measured and a check of the signal-to-noise ratio is performed. Peaks smaller than three times the rms amplitude of the pre-event noise are rejected.

Regressions are carried out on the time domain bandpass-filtered peak ground velocities, after casting in matrix form the thousands available observations at each sampling frequency. The matrix form is indicated in the following scheme:

$$A_k(f_0, r_{ij}) = SRC_i(f_0, r_{ref}) + SITE_j(f_0) + D(r_{ij}, r_{ref}, f_0) \qquad (1a)$$

where A_k (f_c, r_{ij}) is the logarithm of the observed peak amplitude (j-th station, i-th event) for the k-th waveform band-pass filtered around f_0; D(r_{ij}, r_{ref},f_c) is described with a piecewise continuous function:

$$D(r_{ij}, r_{ref}, f_0) = \sum_{m=1}^{N} L_m(r_{ij}) D_m \qquad (1b)$$

where $L_m(r)$ is a linear function, and D_m is the value of the attenuation function at the hypocentral distance, r.

For stability, the following constraints are applied during the regression analysis:

- D(r = r_{ref}, f) = 0 (r_{ref} = 40 km) (2)

Constraint (2) maps source effects to an arbitrary reference distance. To facilitate comparisons with the results of similar studies elsewhere in Italy (Malagnini et al., 2002), we chose the reference distance to be 40 km.

- $SITE_{STV2}(f) = 0$ (3)

  Because of constraint (3), all site terms are relative to the hard-rock station STV2, that is deployed on gneiss outcrops of the Argentera Massif. The excitation terms, $SRC_i(f_0, r_{ref})$, are also related to this specific reference station.

- A smoothing constraint is also applied to $D(r, r_{ref}, f)$:

  $D_{j-1}(f) - 2D_j(f) + D_{j+1}(f) = 0$ (4)

  Equation (4) describes a minimum roughness constraint, which equals a null-second derivative when the nodes are evenly spaced.

Duration of the ground motion is calculated for each seismogram. At each frequency, duration is defined as the length of the time windows comprising the 5% - 75% of the energy following the S-wave arrivals on the filtered seismograms (figure 6). We estimate the duration of each seismogram, and check its reliability by comparing the observed peak motion to its RVT prediction (via the Stochastic Model SIMulation code - SMSIM - Boore, 1996).

Results

Attenuation model for the region

We modeled the empirical estimates of the peak amplitudes, as a function of hypocentral distance in each frequency band. Since the crustal attenuation is described as a combination of geometrical spreading g(r), and a frequency-dependent crustal attenuation parameter, Q(f), $D(r, r_{ref}, f)$ can be described as following equation:

$$D(r, r_{ref}, f_c) = \log g(r) - \log g(r_{ref}) - \frac{\pi f_c (r - r_{ref})}{\beta Q_0 (f / f_{ref})^{\eta}} \log e ; \quad (5)$$

The search on the parameters Q_0 and η in: $Q(f) = Q_0(f / f_{ref})^{\eta}$ (f_{ref}=1.0 Hz), and on the geometrical spreading function g(r) in (5) yielded:

$$Q(f)=310\, f^{0.20} \qquad (6)$$

$$g(r) \propto \begin{cases} r^{-0.9} & r \le 40\,km \\ r^{-0.5} & 40 < r \le 100\,km \\ r^{-0.9} & 100 < r \le 120\,km \\ r^{-0.5} & r > 120\,km \end{cases} \qquad 0.5 \text{ Hz} \le f \le 1.0 \text{ Hz} \qquad (7)$$

$$g(r) \propto \begin{cases} r^{-0.9} & r \le 40\,km \\ r^{-0.5} & r > 40\,km \end{cases} \qquad f > 1.0 \text{ Hz} \qquad (8)$$

Although (in the log log space) equation (7) describes a quadri-linear geometrical spreading for the lower frequency band (0.5 Hz ≤ f≤1.0 Hz), the high-frequency term (f≥1.0 Hz) given by equation (8) is simply bilinear, with a body-wave-like spreading (g(r)~1/r) out to 40 km (hypocentral distance), and cylindrical spreading (g(r)~1/√r) beyond 40 km. Figure 7 shows the empirical function describing the crustal attenuation in the Western Alps, as obtained from the regressions on the peak values of the band-pass filtered ground velocities. Color curves represent the empirical estimate of the term $D(r,r_{ref},f)$ at various frequencies, while the black curves in the background represent theoretical predictions obtained using equations (6), (7), and (8).

Comparisons with results of similar studies in Switzerland, and in the eastern Alps;

Two different comparisons are appropriate for our results: i) with the results by Bay et al. (2003) on Switzerland, ii) with the results by Malagnini et al. (2002) on the eastern Alps. Comparisons can be about the crustal attenuation term $Q(f)=Q_0 f^{\eta}$, and/or with the high-frequency geometric attenuation g(r), which contains information about the crustal velocity structure.

i. Switzerland was recently investigated by Bay et al. (2003). After using the same method as in

this study, they indicated the following crustal parameters: $Q(f)=270\ f^{0.50}$. Their results are more similar to the ones obtained for the eastern Alps than for the ones of this study. A complex, quadri-linear (in a log log space) geometrical spreading was proposed for Switzerland, where spherical propagation characterizes short distances (less than 50 km), cylindrical propagation are supposed to take over beyond 100 km, and a complex pattern exists between the two crossover distances. A deeper Moho beneath the Swiss Alps explains the farther transition to cylindrical propagation, and the large crustal shortening experienced by the central Alps during their tectonic history has probably leaded to a more complex average 1-D vertical layering than for the western Alps.

ii. For the eastern Alps, Malagnini et al. (2002) found a more complex apparent geometrical spreading than in northwestern Italy, with branches steeper than 1/r (almost as steep as $1/r^2$) at intermediate distances, that may be interpreted as shadow zones due to velocity inversions at depth. The nature of this peculiar behavior is related to the compressive tectonic setting of the eastern Alps, where the present tectonics acts via low-angle, northward-dipping thrust faults. The anelastic attenuation term in the region, $Q(f)=260\ f^{0.55}$, is characterized by a similar Q_0 than in the western Alps, but by a much stronger frequency dependence. At frequencies around 1.0-2.0 Hz, differences in the anelastic attenuation are insignificant, but the high-frequency wave propagation is apparently a lot more efficient in the eastern Alps. The coupled geometric attenuation function, though, averages out the apparent attenuation of the peak amplitudes, leading to an overall similarity between the absolute attenuation of the peak values. Only the higher frequencies in the band of interest attenuate in substantially different ways in the two regions.

Source excitation spectra

The empirical excitation terms $SRC_i(f_0, r_{ref})$ are modeled using the Brune (1970) spectral model,

then they are "propagated" to the reference hypocentral distance of 40 km (eqs. 5, 6, 7, 8). Figure 8 shows the inverted excitation terms obtained for the peak filtered amplitudes (black diamond linked by thin black lines). The thick gray lines in the figure refer to the theoretical excitation terms obtained by using equations (5), (6), (7), (8), (9), (10), and (11) at various moment magnitudes:

$$exc(f, r_{ref}) = s(f, M_W) g(r_{ref}) \exp\left[-\frac{\pi r_{ref}}{\beta Q_0 (f / f_{ref})^{\eta}} \right] V(f) \exp(-\pi f \kappa_0) \tag{9}$$

where $V(f) = 1.0$:

$$s(f, M_W) = K \frac{M_o}{4\pi\rho\beta^3 1000} (2\pi f) S(f) \tag{10}$$

$$K=0.24 \tag{11}$$

The constant parameter K in equations (10) and (11) (Boore 1983, Boore 2000, Atkinson and Boore 1995) takes into account: i) the radiation pattern, log- or rms-averaged over a suitable range of azimuth and take off angles ($<R_{\Theta\Phi}>$, Boore and Boatwright, 1984); ii) the amplification due to the free surface, and iii) the partitioning of energy into horizontal components. Although we have no information to separate each contribution, we have the necessity to calibrate K to the specific dataset using independent information (Herrmann and Malagnini, 2004). We thus defined this parameter on our dataset using independent and stable moment magnitudes given in a recent source study on the same dataset (Morasca et al. 2004).

The reference distance has been selected so that it is far enough from source to minimize depth errors, but not too far that reflected crustal arrivals complicate the motion (Herrmann and Malagnini, 2004). In table 2 we report the numerical values of all parameters of the spectral model. The term, $\exp(-\pi\kappa_0 f)$, is used to model the decay of the high-frequency band in the empirical excitation spectra. In our formulation, κ_0 is a distance-independent site term, related to the effective anelastic absorption at shallow depths beneath station STV2 of the vertical ground motion carried by S-waves (the only station and component of the ground motion constrained to be zero during the regressions).

Since the stress parameter in the Brune model trades off with κ_0, we need to calibrate κ_0, and then to quantify the stress parameter $\Delta\sigma$ by best-fitting the excitation terms. As seen in figure 9, the high-frequency spectral amplitudes of small events are essentially dominated by the effect of κ_0 and for large events, a strong tradeoff exists between κ_0 and the stress parameter $\Delta\sigma$. We estimated κ_0=0.012 sec by fitting the shape of the average spectrum of about 130 small earthquakes. The stress drop, $\Delta\sigma$=50MPa, is thus calculated from the largest event in our data, M 5.1 by fixing κ_0=0.012 sec.

ρ	2.8 g/cm3
β	3.5 km/sec
$\Delta\sigma_{(Mw=4.8)}$	50 MPa
f_c	4.9 X $10^6\beta(\Delta\sigma/M_0)^{1/3}$ Hz
κ_0	0.012 sec
$\nu(f)$	1.0

Table 2 Parameters of the Brune Spectrum used to compute the theoretical excitation terms

Site terms and H/V ratios

Vertical and horizontal site terms obtained from our regressions are shown in figure 10. Since we forced the vertical site term at station STV2 to be zero during the inversions, all individual (vertical and/or horizontal) site terms given here are relative to the STV2 vertical-component motion. Figure 10 also reveals that the entire set of site terms is characterized by small fluctuations with respect to the vertical STV2, except for station MONE, which shows a substantial amplification on the horizontal components of the ground motion, in the 2-10 Hz frequency band. The empirical site term, $SITE_j(f)$ has the following meaning:

$$10^{SITE_j(f)} = \frac{V_j(f)\exp(-\pi\kappa_{0j}f)}{V_{STV2}(f)\exp(-\pi\kappa_{STV2}f)} \quad (12)$$

The regional high-frequency term:

$$\exp(-\pi\kappa_0 f) \approx V_{STV2}(f)\exp(-\pi\kappa_{STV2}f) \quad (13)$$

$V_j(f)\exp(-\pi\kappa_{0j}f)$; $V_j(f)$ is the site-specific elastic response, and $\exp(-\pi\kappa_{0j}f)$ is the distance-independent, site-specific, high-frequency anelastic attenuation. From a visual inspection of the figure 10, we see that the error bars tend to be very large at frequencies below 1.0 Hz. The same result is obtained for the empirical attenuation $D(r,r_{ref},f)$ in figure 7, for which large error bars are observed for frequencies $f \leq 1.0$ Hz.

We also calculated the individual horizontal-to-vertical ratios from each one of the individual empirical terms (figure 11). A stable behavior characterizes all site terms, with a slight increase of the ratios for increasing frequencies. The H/V ratios can be used, together with the source, propagation and vertical site terms, in order to compute the expected horizontal ground motion at each station.

Automatic Moment Magnitude Calibration

Through a completely automatic procedure, Malagnini et al. (2004) use the regionally-calibrated attenuation parameters obtained from similar regressions in the eastern Alps in order to compute corrected moment-rate spectra for small and moderate earthquakes. Similarly, in this paper we compute seismic moments from the rms-average of the flat portion of the corrected moment-rate spectra of the events in the data set, and thus the moment magnitudes for all the events in our data set.

Independent values of M_W were also computed by Morasca et al. (2004) for all the events in the data set, based on measurements taken on the seismic coda, that are much less sensitive to the source radiation pattern and to 3D-heterogeneities than our direct phase measurements, we calibrated the constant K on their moment magnitudes. Using K=0.24 in (10), our results were comparable to the ones of Morasca et al. (2004) (figure 12). This means that, in the Western Alps, the effect of complex structures, lateral heterogeneities, and irregularities close to the surface, have an important influence on the average values described by K. For this parameter, Malagnini et al. (2004) used the canonical value: K=0.89.

Finally, figure 13 shows our seismic moments versus the local magnitudes computed by Spallarossa et al. (2002). The thick black line is the result of the data least-square fitting. It is described by the following moment versus magnitude relationship:

$$\log M_0 = (0.92 \pm 0.01) M_L + (17.676 \pm 0.007) \quad (14)$$

It is worth mention that there is no specific physical meaning for the relationship above to be linear, unless within a very narrow magnitude range.

The magnitude range of confidence is between $0.5 \leq M_L \leq 5.1$. We also compared our results with the relations of Scherbaum and Stoll (1983) for the Swabian Jura, SW Germany ($\text{Log } M_0 = 1.0\ 5\ M_L + 16.86$, $1.0 \leq M_L \leq 4.5$), Granet and Hoang Trong (1980) for Friuli, NE Italy ($\text{Log } M_0 = 0.83\ M_L + 17.40$, $0.8 \leq M_L \leq 3.0$), and Lanza et al. (1999) for the Southwestern sector of Alps ($\text{Log } M_0 = 1.06\ M_L + 16.94$, $1.5 \leq M_L \leq 4.5$). Our relationship (14) shows a clear DC-shift relative to these studies. Scherbaum and Stoll's moments are based on 5 sites over approximately 1 km of sediment, and they computed moments from the 1-10 Hz bandpass, with no corrections for site amplifications. Local magnitudes derived by Spallarossa et al. (2002) are calibrated on the same area analyzed in this study. The relationship by Lanza et al. (1999) was calculated by using data recorded during two swarms occurred in 1993. Our dataset includes a large number of events extending over the entire area of the western Alps, allowing us to get more stable results. Granet and Hoang Trong (1980) provide no information on their local magnitude computation.

Predicting the ground motion at large magnitudes

In this section, we produce quantitative predictions of strong ground motion for earthquakes characterized by magnitudes up to M_w 6, that are outside the range covered by the present data set. The lack of large events in the data set forces us to extrapolate the predictions to high levels of ground shaking, although the large amount of recordings from small earthquakes provides strong constraints on regional wave propagation. In fact, the estimated Peak Ground Acceleration (PGA) as a function of epicentral distance (figure 14) are obtained based on RVT, as implemented by

Boore (1996), by using the attenuation parameters and the empirical duration function that are given in this study.

The predicted peak values are compared with those by Sabetta and Pugliese (1996), who regressed a very small accelerometric data set of strong-motion waveforms from events occurred in the Apennines, in Sicily, and in the eastern Alps. Comparisons are also given with the results by Ambraseys et al. (1996), who regressed the strong-motion data from the European accelerometric data set.

Since Sabetta and Pugliese (1996) refer to epicentral distance and those by Ambraseys et al. (1996) to fault distance, we should not compare different distance metrics. However, other studies used this approximation (Malagnini et al. 2002), and considered it acceptable for the purpose of a mere comparison.

The comparison between different estimates of PGA for moment magnitudes M_w 5 and 6 (figure 14) shows interesting differences: except at small distances, our predicted ground motions are generally lower than both predictions by Sabetta and Pugliese (1996) and Ambraseys (1996).

Regional differences in the attenuation of seismic waves should not be neglected because reflect differences in the geologic structures and in the thermal histories. For example, the Apennines are characterized by a strong attenuation, $Q(f)=130f^{0.1}$ (Malagnini et al. 2000a), which is caused by the presence of a high fracture density and consequently of large fluid/volatile flows in the crust; the attenuation of the seismic waves is lower in more stable portions of the crust, like that beneath Friuli (eastern Alps), $Q(f)=260f^{0.55}$ (Malagnini et al. 2002). The western Alps (in this study), where crystalline basement is shallower, has also a low-attenuation crust, $Q(f)=310f^{0.2}$. Differences in wave propagation can thus be easily linked with the geologic and tectonic settings of the areas and play a key role in hazard studies.

Spectral velocities are also compared with results of regressions carried out by Sabetta and Pugliese (1996) and by Ambraseys et al (1996) for fault/epicentral distances of 15 and 60 km (figure 15). As for the PGA curves, our pseudo-velocity spectra are systematically lower than those obtained by

Ambraseys et al. (1996) and Sabetta and Pugliese (1996).

Conclusions

The regional attenuation for the earthquake-induced ground motion in the western Alps was investigated using a large dataset of seismograms from the background seismicity, recorded by the Regional Seismic network of Northwestern Italy (RSNI).

A suite of regressions was performed at a set of frequencies, between 0.5 and 14.0 Hz, on the logarithms of the peak values of narrowband-filtered versions of the original seismograms. As a result, for each central frequency of the narrowband filters, we obtained: i) empirical estimates of the regional propagation within the distance range sampled by the data set; ii) a suite of excitation terms (one for each earthquake included in the specific regression); iii) a set of site terms (one for each site included in the regression).

A modeling effort was undertaken in order to produce an effective model for: i) the wave propagation in the region, and, ii) the excitation terms. As far as the crustal propagation is concerned, within hypocentral distances of 160 km and for frequencies up to 1.0 Hz, we use a quadri-linear geometrical spreading, whereas a simpler bilinear function properly describes the empirical results at higher frequencies. The parameter $Q(f)= 310f^{0.20}$, that indicates a fairly stable region, is used for taking into account the anelastic attenuation. By comparing our results with the ones obtained in similar studies (Bay et al., 2003; Malagnini et al., 2002), we observed, around 1.0 Hz, similar attenuation characteristics for the western Alps, the eastern Alps, and for Switzerland. A much lower attenuation at high frequency characterize the eastern Alps, whereas the entire frequency band of engineering interest is affected by a much stronger attenuation in the Apennines.

The empirical excitation terms obtained from the regressions require κ_o=0.012 sec, and a maximum value for the stress parameter of 50 MPa. The mentioned parameter is to be referred to a moment magnitude $M_w \approx 5$, and to the reference station STV2, located on hard rock.

About the geometrical spreading function needed to reproduce the empirical attenuation of seismic waves in the western Alps, it reflects the average 1-D structure of the crust in the region, in terms of the depths of the most important interfaces, and of the impedance contrasts across them. Local earthquake tomography reveals the complexity of the three-dimensional lithospheric structure in the region (Kissling, 1993, Kissling and Spakman 1996, Paul et al. 2001), suggesting the presence of asymmetric crustal roots, and of anomalous high-velocity features, like the Ivrea body (a wedge of Adriatic upper mantle, Paul et al., 2001).

The role of the three-dimensional complexities in determining the attenuation functional forms proposed in this study is still unclear: if the source-receiver geometry allows systematic effects, these may lead to changes in the apparent geometrical spreading function. If no systematic effects exist, lateral heterogeneities may only increase the amplitudes of the residuals. For the region investigated here, a preliminary analysis of the 2-D distribution of the residuals excludes systematic distributions of the residuals along specific paths. Moreover, the relative simplicity of the high-frequency attenuation relationships suggests the absence of systematic effects on the apparent attenuation itself.

Differences in the predicted ground motions from our relationships and the existing ones (e.g., Ambraseys et al., 1996; Sabetta and Pugliese, 1996) are because our results are based solely on information obtained from the specific region. The cited studies were only carried out on heterogeneous data sets made of recordings of events within the entire Italian territory or even within Europe. On the other hand, differences in the estimated peak ground accelerations from different studies in different tectonic and geologic zones (the Apennines, the eastern and western Alps) show the importance of studying on the basic factors (the source scaling, regional attenuation and site conditions) and their influences to the seismic hazard.

The attenuation parameters obtained here allowed us to correct the recorded displacement spectra even for very small earthquakes, and to automatically compute seismic moments and moment magnitudes. Results have been validated through a comparison with stable estimates of moment

magnitude obtained for the same dataset by Morasca et al. (2004). A systematic DC-shift between our results and those from other studies (Scherbaum and Stoll, 1983; Lanza et al., 1999; Granet and Hoang Trong, 1980) strongly suggests that magnitudes must be computed using relationships calibrated on the region of interest.

ACKNOWLEDGMENTS

This work was performed under the auspices of the Italian Ministry of University and Scientific Research (MIUR), under FIRB contract no RBAU013NRZ. Additional support was obtained in the framework of the project "Probable Earthquakes in Italy from Year 2000 to 2030", funded by the Gruppo Nazionale per la Difesa dai Terremoti.

REFERENCES

Akinci, A., Malagnini, L., Pino, N. A., Scognamiglio L., R. B. Herrmann, and H. Eyidogan. High-Frequency Ground motion in the Erzincan Region, Turkey: Interferences from small Earthquakes. *Bull. Seism. Soc. Am.* **91**, n 6, 1446-1455, 2001

Ambraseys, N. N., Simpson, K. A., and J. J. Bommer . Prediction of horizontal response spectra in Europe. *Earthquake eng. Struct. Dyn.* **25**, 371-400, 1996

Atkinson, G. M. and D. M., Boore . Ground Motion Relations for Eastern North America. *Bull. Seism. Soc. Am.,* **85**, n 1, 17-30, 1995.

Atkinson, G. M. and Silva, W. J. An Empirical study on earthquake source spectra. *Bull. Seism. Soc. Am.,* 87, 97-118, 1997.

Bay, F., Fäh D., Malagnini, L. and D. Giardini. Spectral Shear-Wave Ground-Motion Scaling in Switzerland. *Bull. Seism. Soc. Am.* **93** (1), 414-429, 2003.

Bodin, P., Malagnini, L., Akinci, A. Ground motion scaling in the Kachchh basin, India, deduced fromaftershocks of the 2001 Mw 7.6 Bhuj earthquake. *Bull. Seism. Soc. Am. (in press),* 2004.

Boore, D. M. Stochastic simulation of high-frequency ground motions based on seismological models of the radiated spectra. *Bull. Seism. Soc. Am.* **73**, n 6, 1865-1894, 1983.

Boore, D. M. SMSIM – Fortran programs for simulating ground motion from earthquakes: *version 1.0. U. S. Geological Survey open –file report* 96-80-A, 73, 1996.

Boore, D. M. Prediction of ground motion using the stochastic method. Aki Symposium, PAGEOPH, v **1**.1, 2000

Boore, D. M., and J. Boatwright. Average Body-wave Radiation Coefficients. *Bull. Seism. Soc. Am.* **74**, 1615-1621, 1984.

Boore, D. M., Joyner, W. B., Fumal, E. T. Equations for estimation horizontal response spectra and peak acceleration from western North American earthquakes: a summary of recent work. *Seis. Res. Lett.* **68**, 1, 129-154, 1997.

Brune, J. N. Tectonic stress and the spectra of seismic shear waves from earthquakes. *J. Geophys. Res.,* **75**, 4997-5009, 1970.

Buness, H., Giese, P., Hirn, A., Nadir, S., Scarascia, S., Crustal structure derived from seismic refraction between Southern Alps and the Ligurian Sea. *Proceeding of the Sixth Workshop on the EGT Project: data compilation and synoptic interpretation, edited by R. Freeman and St. Mueller (European Science Foundation, Strasbourg, France),*165-167, 1990.

Campbell, W. K. Empirical near-source attenuation relationships for horizontal and vertical components of peak ground acceleration, peack ground velocity, and pseudo absolute acceleration response spectra. *Seism. Res. Lett*., **68**, 1, 128-154, 1997.

Cartwright, D.E., and M. S. Longuet-Higgins. The statistical distribution of the maxima of a random function. *Proc. Roy. Soc. London* **A 237**, 212-232, 1956.

Castaldini, D. and Panizza, M. Inventario delle faglie attive tra i fiumi Po e Piave e il Lago di Como (Italia settentrionale). Il Quaternario **4**, 605-611, 1991

Cattaneo, M., Augliera, P., Parolai, S., and D. Spallarossa. Anomalously deep earthquakes in northwestern Italy. *Journal of Seismology,* **3** (4): 421-435, 1999.

Castellarin A. Alps-Appennines and Po Plain-frontal Appennines relations. In: *Vai G.B. and Martini I.P., Eds, Anatomy of an orogen: the Apennines and adjacent Mediterranean basins.*

Kluwer Academic Publishers, Dordrecht-Boston-London, 177-196, 2001.

CNR-PFG. Neotectonic Map of Italy. Quaderni de La Ricerca Scientifica, 114, 1987

Dal Piaz G.V. Plate tectonics and mountain building: the Alps. Historical review and personal comments. In: *Ranalli G. (Ed): Proceedings VIII Summer School Earth & Planetary Sci., Plate Tectonics: The first twenty-five years, pp. 171-251, Univ. Siena 1994* , 1995.

Dewey, J. F., Pitman, W. C., Ryan, W.B.F. and Bonnin, J. Plate tectonics and the evolution of the Alpine System. *Bulletin of the Geo. Soc. of Am.* **84**; pp.3137-3180, 1973.

Di Stefano, R., Chiarabba, C., Lucente, F. and A., Amato. Crustal and uppermost mantle structure in Italy from the inversion of P-wave arrival times: geodynamic implications. Geophys. J. Int. **139**, 483-498, 1999.

Eva, E., and S. Solarino. Variations of stress directions in the western Alpine arc. *Geophis. J. Int.* **135**,438-448, 1998.

Ferrari, G., The 1887 Ligurian earthquake: a detail study from contemporary scientific observations. Tectonophysics, 93, pp.131-139, 1991.

Galadini, F., Meletti, C. and Vittori, E., Major active faults in Italy: available surface data. Netherlands Journal of Geosciences, 80, 273-296, 2001.

Giglia, G., Capponi, G., Crispini, L., and M. Piazza. Dynamics and seismotectonics of the West-Alpine arc. *Tectonophysics* **267**, 143-175, 1996.

Granet, M., and P., Hoang Trong. Some medium properties at Friuli (Italy) from amplitude spectrum analysis: a possible change in time or in space. *Tectonophysics* **68**,16-182, 1980.

Herrmann, R.B., Dutt, J., High frequency vertical ground motion in the Pacific Nothwest using PNSN data. *Seism. Res. Lett.,* **70**, Issue 2, pp.216, March/April 1999.

Herrmann, R. B. and L. Malagnini. Interpretation of High Frequency Ground Motion from Regional Seismic Network Observations, *Bull. Seism. Soc. Am*. (*submitted*), 2004.

Kissling, E. Deep structure of the Alps – what do we really know? *Physics of the Earth and Planetary Interiors*, **79**, 87-112, 1993.

Kissling E. and W., Spakman. Interpretation of tomographic images of uppermost mantle structure: examples from the western and central Alps. *J. Geodynamics*, **21**, 1, 97-111, 1996.

Jeon, Y. S. and R. B. Herrmann. High frequency Earthquake ground motion Scaling in Utah and Yellowstone, *Bull. Seism Soc. Am., (in review)* 2004

Lanza, V., Spallarossa, D., Cattaneo, M., Bindi, D., P. Augliera. Source parameters of small events using constrained deconvolution with empirical Green's functions. *Geophis. J. Int.* **137**,651-662, 1999.

Malagnini, L., Akinci, A., Herrmann, R. B., Pino, N. A. , and L. Scognamiglio Characteristics of the ground motion in northeastern Italy. *Bull. Seism. Soc. Am.,* **92**, 6, 2186- 2204, 2002.

Malagnini, L., and R.B., Herrmann., Ground motion scaling in the region of the Umbria-Marche earthquake of 1997. *Bull. Seism. Soc. Am.,* **90**, 1041-1051, 2000.

Malagnini, L., Herrmann, R.B., and M. Di Bona., Ground motion scaling in the Apennines (Italy). *Bull. Seism. Soc. Am.,***90**, 1062-1081, 2000a.

Malagnini, L., Herrmann, R.B., and K. Koch., Regional Ground-Motion Scaling in Central Europe. *Bull. Seism. Soc. Am.,* **90**, 1052-1061, 2000b.

Malagnini, L., Mayeda, K., Akinci, A., Bragato, P. L. Estimation Absolute Site Effects. *Bull. Seism. Soc. Am.,* 2004 *(in press).*

Morasca, P., Mayeda K., Malagnini, L. and W. R Walter. Coda Derived Source Spectra, Moment Magnitudes, and Energy-Moment Scaling in the Western Alps. *Geophysical Journal International,* 2004 (*in review*)

O'Connell, R.J., and Budianski, B., Seismic velocities in dry and saturated cracked solids. *J. Geophys. Res.,* **79**, 5412-5426, 1974.

Ortega, R., Herrmann, R. B. and L. Quintinar. High frequency earthquake ground motion scaling in central Mexico between 0.7 and 7 Hz. Bull. Seism. Soc. Am., **93**, 397-413, 2003.

Paul, A., Cattaneo, M., Thouvenot, F., Spallarossa, D.,Béthoux, N., and J. Fréchet A three-dimensional crustal velocity model of the southwestern Alps from local earthquake tomography. *J.*

Geophis. Res .**106**, B9, 19,367-19,389, 2001.

Polino, R., Gosso, G. and Dal Piaz, G. V. Un modello attualistico sulla genesi delle Alpi. Memorie della Società Geologica Italina **45**, 71-75, 1990.

Pino, N.A. Malagnini, L., Akinci, A., Scognamiglio, L., Herrmenn, R.B., Stavrakakis, G., and G. Chouliaras. Ground Motion Scaling relationships for mainland Greece and Crete. *Seism. Res. Lett.,* **72**, 258, 2001.

Raoof, M., Herrmann, R.,B., and L. Malagnini. Attenuation and excitation of three-component ground motion in Southern California. *Bull. Seism. Soc. Am.* **89**, 888-902, 1999.

Sabetta, F., and A. Pugliese. Estimation of response spectra and simulation of nonstationary earthquake ground motion. *Bull. Seism. Soc. Am.* **86**, 337-352. 1996.

Sadigh, K., Chang, C. Y., Egan, J. A., Makdisi, F., Youngs, R. R. Attenuation relationship for shallow crustal earthquakes based in California Strong Motion Data. *Seism. Res. Lett.,* **68**, 154-180, 1997.

Scherbaum, F., and D. Stoll. Source parameters and scaling laws of the 1978 Swabian Jura (southwest Germany) aftershocks. *Bull. Seism. Soc. Am.,* **73**, 1321-1343, 1983.

Scognamiglio L., Malagnini, L., A. Akinci. Ground Motion scaling in Eastern Sicily (Italy). *Bull. Seism. Soc. Am.* (*submitted*), 2004.

Spallarossa, D., Bindi, D., Augliera, P., and M. Cattaneo. An M_L scale in Northwestern Italy. *Bull. Seism. Soc. Am.,* **92**, 6, 2205-2216, 2002.

Sue, C., Thouvenot, F., Fréchet, J., and P. Tricart. Earthquake analysis reveals widespread extension in the core of the Western Alps. *J. Geophys. Res.,* **104**, 25611-25622, 1999.

Sue, C., Tricart, P. Late-Alpine brittle extension above the Frontal Pennine Thrust near Brian on, Western Alps. *Eclog. Geol. Helv., 92,171-181,* 1999.

Yazd , M. R. S. Ground motion studies in the southern Great Basin of Nevada and California. *Ph. D. Dissertation,* Saint Louis University, 1993.

FIGURE CAPTIONS

Figure 1 - Events and stations used in this study. The main seismic activity in the Western Alps is concentrated along an external belt, corresponding to the Crustal Penninic Front (CPF), and along an internal belt, corresponding to the border of the Penninic zone and the Po plain. These seismic belts are connected with a westward translation of the West-Alpine arc and of the Po plain that drives the observed seismicity mechanism (Giglia, et al. 1996, Sue et al., 1999; Sue and Tricart, 1999).

Figure 2 - Characteristics of the data set. A) Distribution of local magnitude (Spallarossa et al. 2002) with respect to hypocentral distance; B) Number of waveforms as a function of local magnitude. The bulk of the events used in this study is characterized by $M_L < 2$, although we included recordings from earthquakes up to $M_L = 5.1$; C) Number of recordings as a function of hypocentral distance; D) Distribution of the event depths, showing that the data set consists mainly of shallow events.

Figure 3 - Seismicity cross-section through the western Alps: the AA′ and CC′ sections try to follow the geometrical structure of the internal and external arcs. The BB′ section shows that focal depths are deeper from west to east.

Figure 4 - Distance coverage for the three components stations used in this study. Each square in this figure represents one distinct three-component seismogram. The spatial sampling of our recordings is fairly homogeneous up to hypocentral distances of about 160 km.

Figure 5 - Signal-to-noise (S/N) ratios calculated in the frequency band 2-11 Hz on a window of 2 seconds.

Figure 6 - Duration distribution for the regional data at different frequencies. It is computed on each individual recording in the data set as the time window bracketing the 5-75 % of the integrated seismic energy that follows the S-wave-onset. Small diamonds indicate individual values of duration; large blue diamonds indicate the L1-norm estimates of the duration computed at a set of

nodes.

Figure 7 - Attenuation functional D(r, f) obtained, for western Alps, from the regressions on the filtered velocities at the frequencies indicated in the figure. Color curves represent the final regression results, the black lines in the background describe the theoretical predictions. Attenuation curves are normalized to zero at the reference hypocentral distance of 40 km. For plotting purposes only we normalized the amplitude decays to 1/r for the term D(r ,r_{ref}, f). Thus, horizontal curves in the figure really decay as 1/r. This choice increases the visual spread of curves at different frequencies, and allows a better sensitivity on the frequency dependence, η, of the attenuation function.

Figure 8 - Comparison between empirical excitation terms obtained from the regressions (indicated by the black diamonds linked by thin black lines) and the predictions from different moment magnitudes, obtained by using the RVT (thick gray lines). Error bars are associated at each empirical term.

Figure 9 - The figure shows the influence of κ_0 on the high-frequency amplitudes of small events, and the tradeoff between κ_0 and the stress parameter for large earthquakes. For this reason, it is necessary first to find estimates of the high frequency parameter, κ_0, on small events spectra, and than, knowing κ_0, of the stress parameter of the larger events.

Figure 10 - Inverted site terms for all the available sites for the regressions over the peak values. We forced STV2 to be zero, during the regressions, because it is on a hard rock location. Each site term refers to STV2. Station MONE shows amplification in the frequency band 2-10 Hz.

Figure 11 - H/V ratio for each station.

Figure 12 – M_w derived from this study are calibrated on M_w(coda) given by Morasca et al. 2004. The values are in excellent agreement when we use K = 0.24.

Figure 13 - Our seismic moments versus M_L for all earthquakes in the data set (gray square symbols). Thick line is the least-squares fit to this data set; thin lines are the relationships for Friuli, NE Italy (Granet and Hoang Trong, 1980) , Swabian Jura, SW Germany (Scherbaum and Stoll,

1983) and SW sector of Alps (Lanza et al. 1999).

Figure 14 - Our estimates of PGA (solid lines),computed for hard rock sites and based on the attenuation and excitation parameters obtained in this study, are compared with the results of the regressions by Sabetta and Pugliese (1996, dashed curves) and Ambraseys et al. (1996) (dotted curves).

Figure 15 - Comparison between our predicted response spectra relative to M =5 and 6 (solid lines) and the empirical results of Sabetta and Pugliese (1996, dashed curves) and Ambraseys et al. (1996, dotted curves), at the fault distances of 15 (top) and 30 km (bottom).

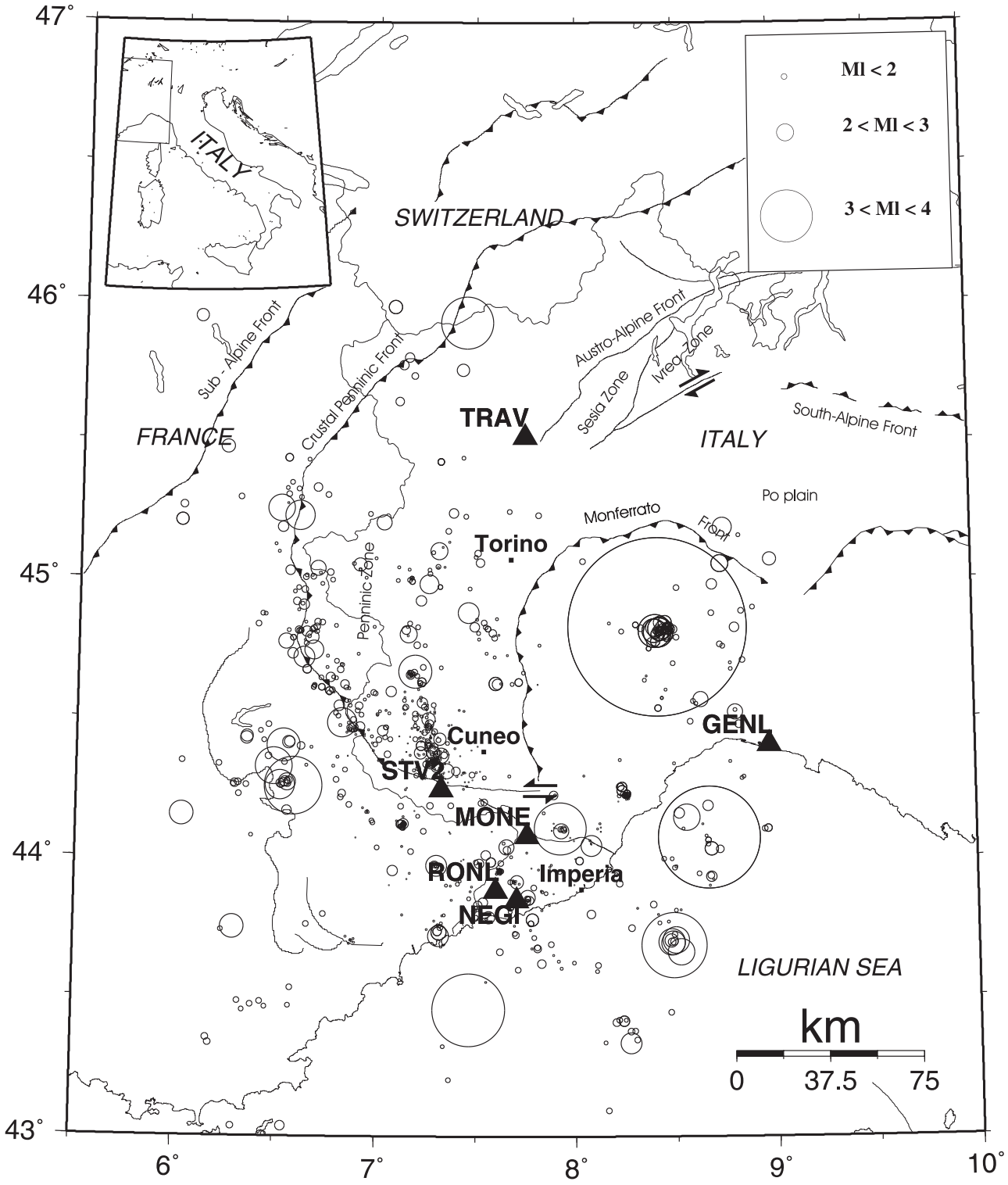
Ml < 2
2 < Ml < 3
3 < Ml < 4
ITALY
SWITZERLAND
FRANCE
ITALY
Sub - Alpine Front
Crustal Penninic Front
Austro-Alpine Front
Sesia Zone
Ivrea Zone
South-Alpine Front
Po plain
Monferrato
Front
Penninic Zone
TRAV
Torino
GENL
Cuneo
STVZ
MONE
RONL
Imperia
NEGI
LIGURIAN SEA
km
0
37.5
75
47°
46°
45°
44°
43°
6°
7°
8°
9°
10°

Figure 1

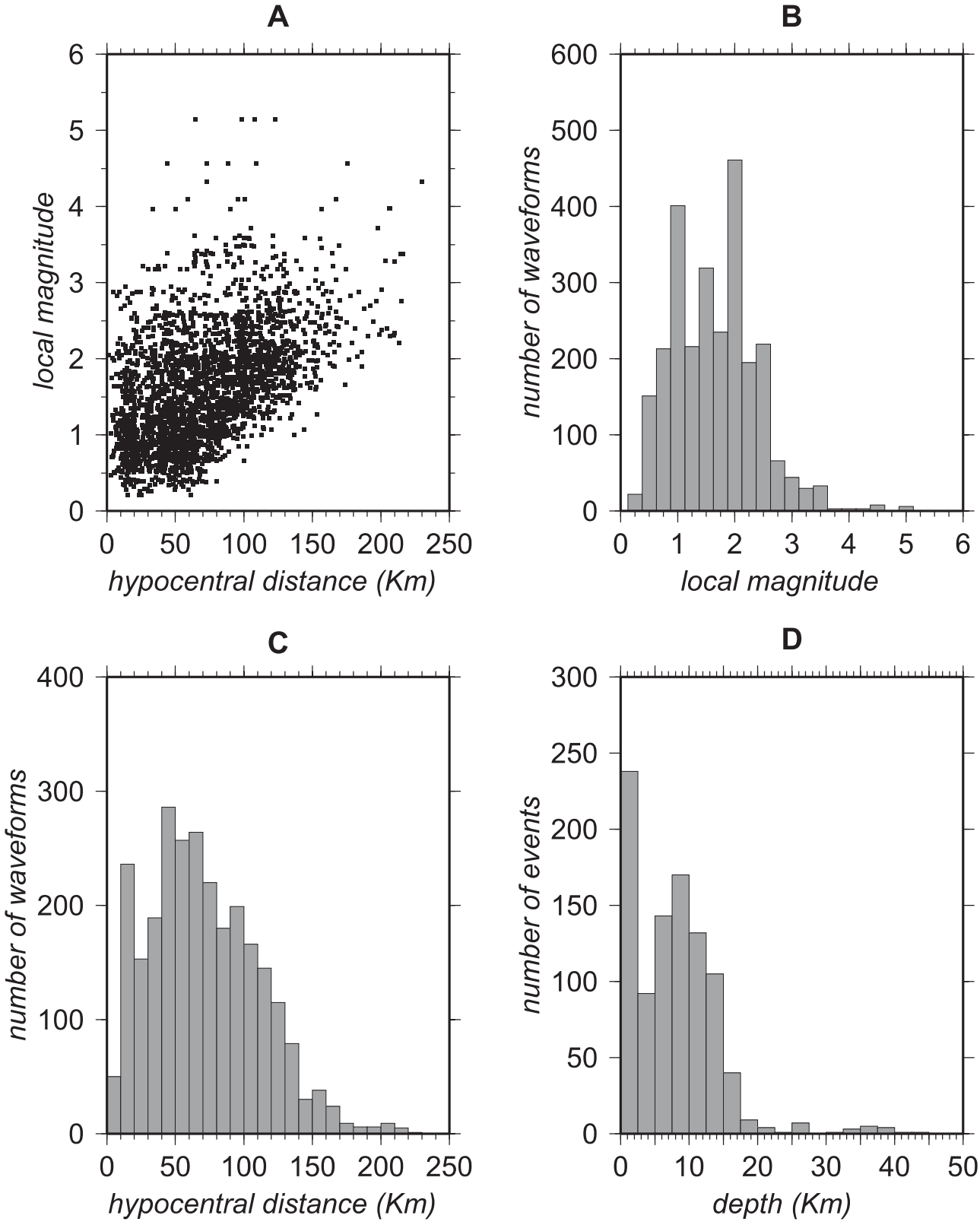
A
local magnitude
hypocentral distance (Km)
B
number of waveforms
local magnitude
C
number of waveforms
hypocentral distance (Km)
D
number of events
depth (Km)

Figure 2

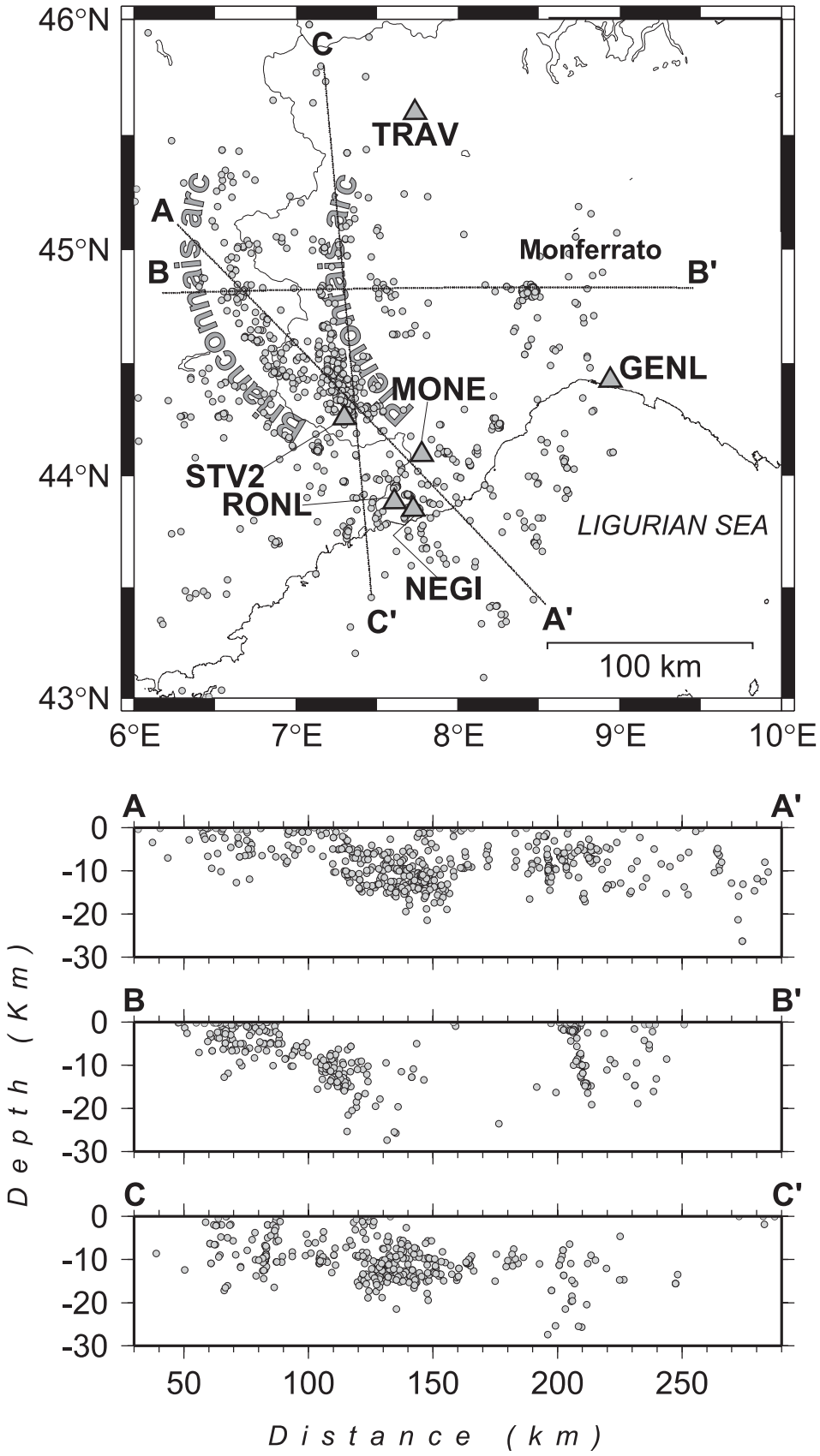
46°N
45°N
44°N
43°N
6°E
7°E
8°E
9°E
10°E
C
TRAV
A
B
Monferrato
B'
GENL
MONE
STV2
RONL
LIGURIAN SEA
NEGI
C'
A'
100 km
Piemontais arc
Apenninic chain
A
A'
B
B'
C
C'
0
-10
-20
-30
50
100
150
200
250
Depth (Km)
Distance (km)

Figure 3

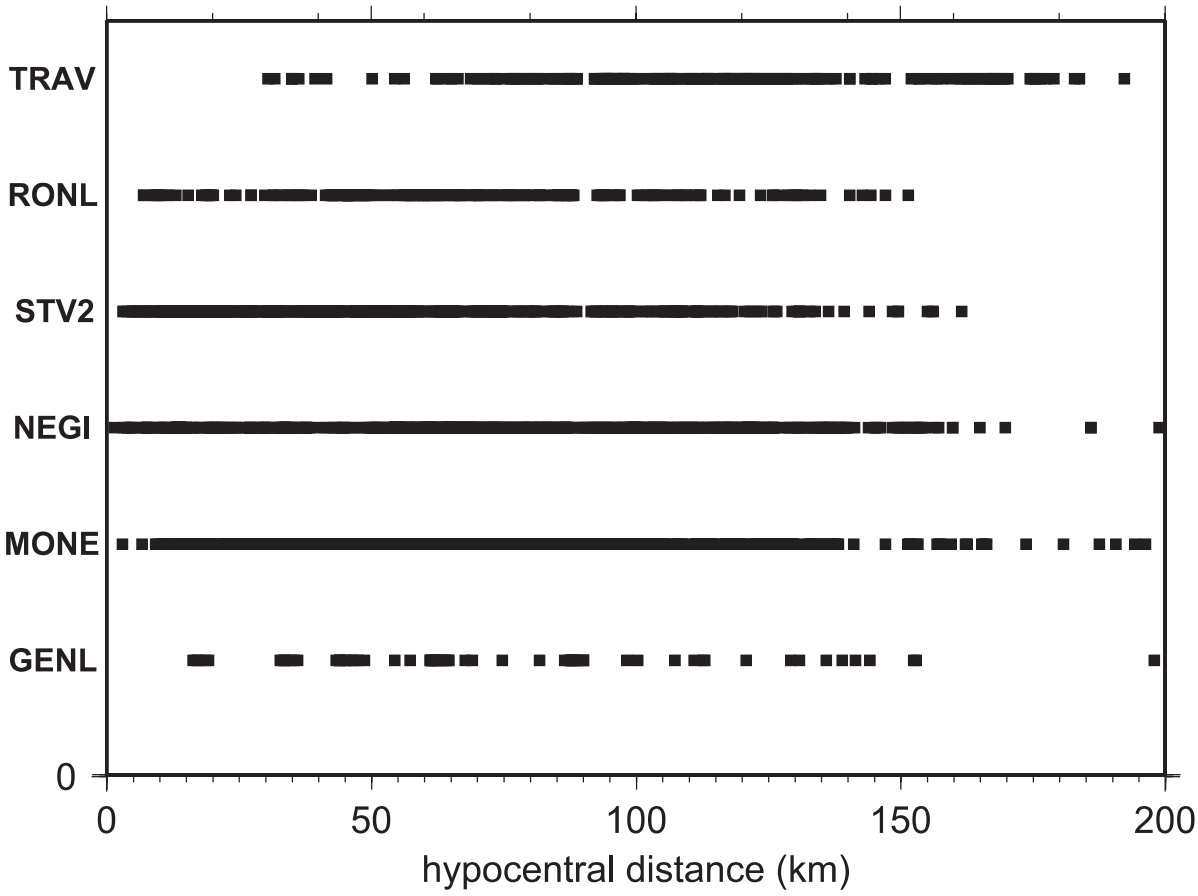
TRAV
RONL
STV2
NEGI
MONE
GENL
0
0
50
100
150
200
hypocentral distance (km)

Figure 4

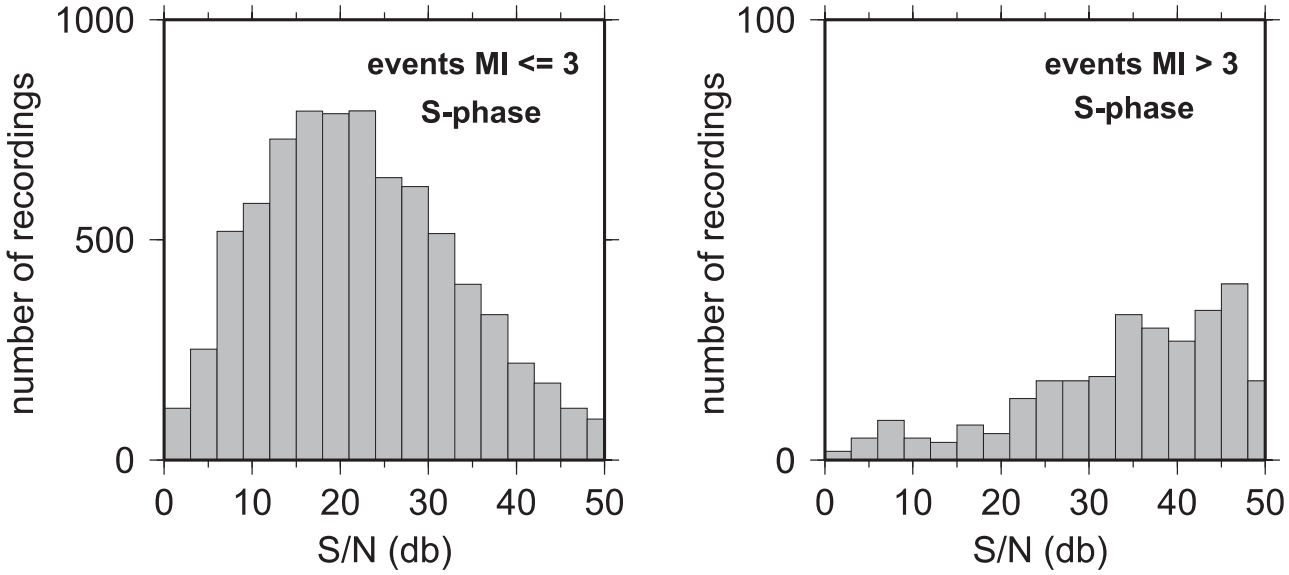
1000
500
0
number of recordings
events MI <= 3
S-phase
0
10
20
30
40
50
S/N (db)
100
0
number of recordings
events MI > 3
S-phase
0
10
20
30
40
50
S/N (db)

Figure 5

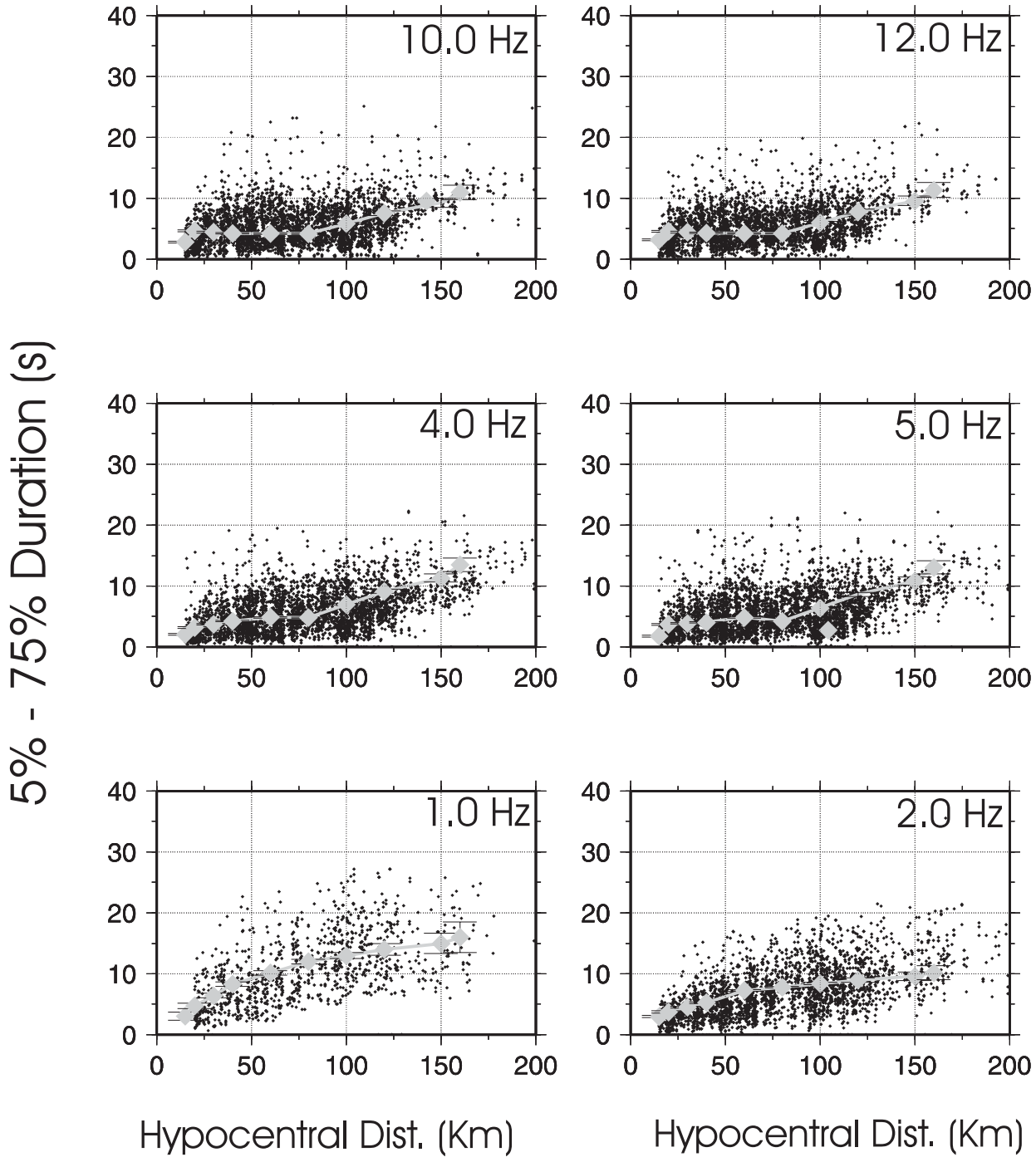
10.0 Hz
12.0 Hz
4.0 Hz
5.0 Hz
1.0 Hz
2.0 Hz
5% - 75% Duration (s)
Hypocentral Dist. (Km)
Hypocentral Dist. (Km)
0
10
20
30
40
50
100
150
200

Figure 6

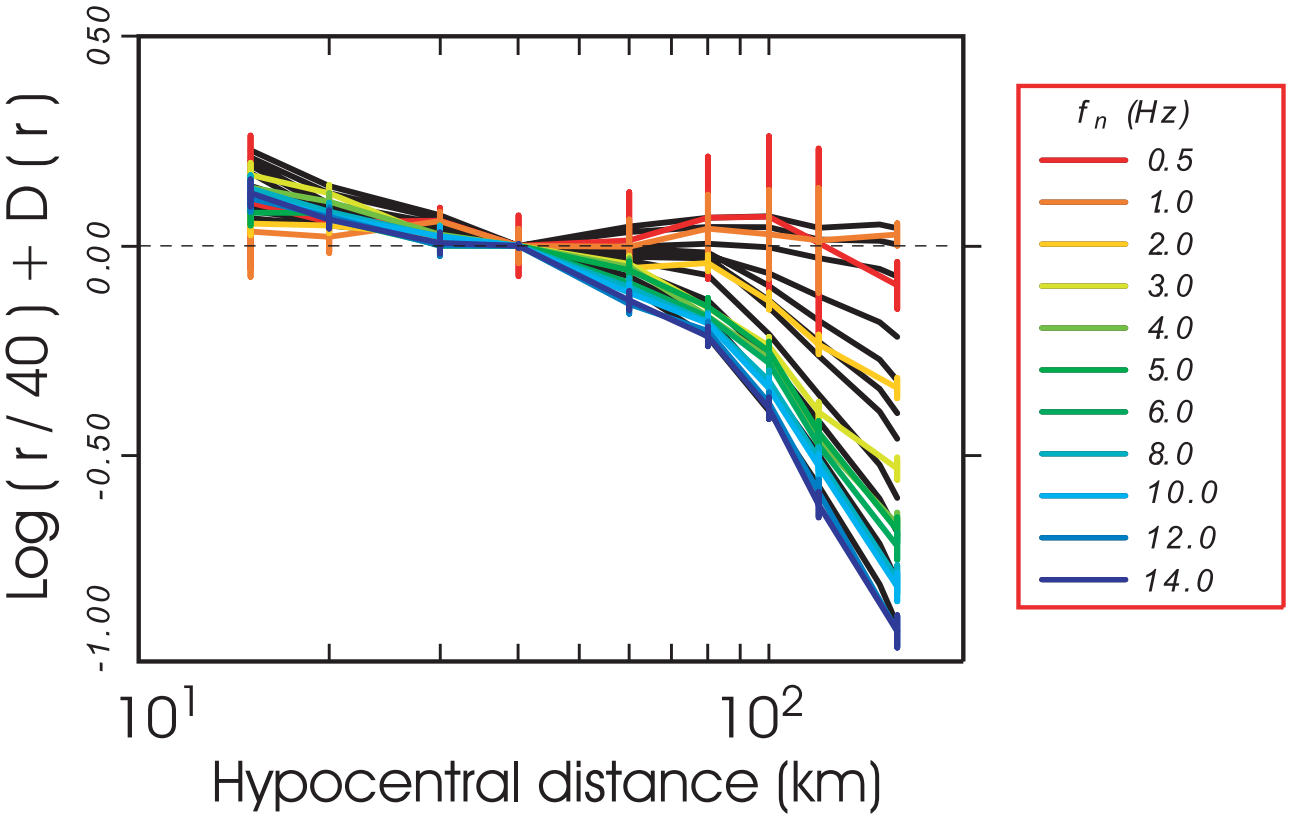
Log (r / 40) + D (r)
050
0.00
-0.50
-1.00
10^1
10^2
Hypocentral distance (km)
f n (Hz)
0.5
1.0
2.0
3.0
4.0
5.0
6.0
8.0
10.0
12.0
14.0

Figure 7

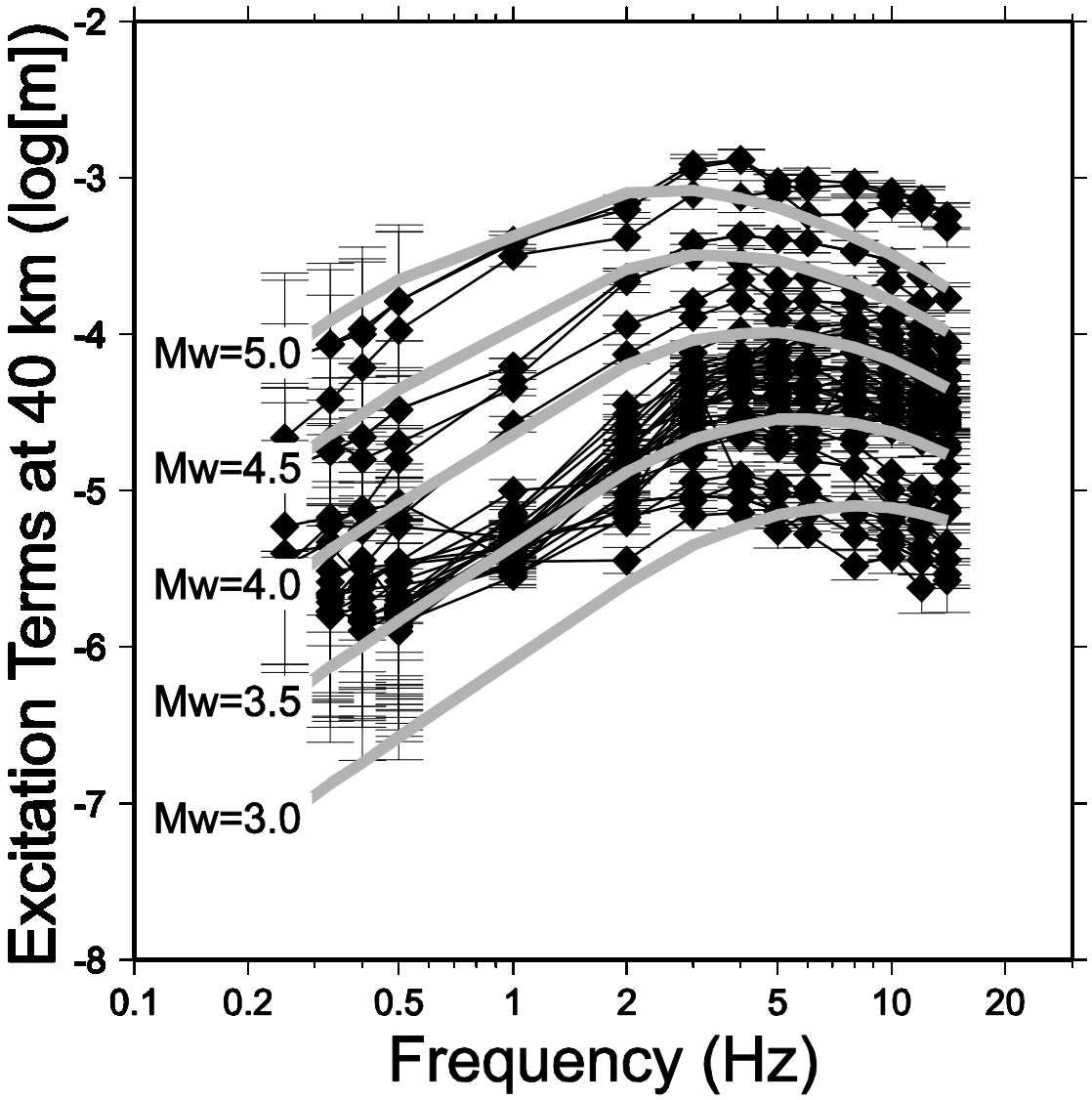
Peak Amplitudes Z-Comp.
Excitation Terms at 40 km (log[m])
-2
-3
-4
-5
-6
-7
-8
Mw=5.0
Mw=4.5
Mw=4.0
Mw=3.5
Mw=3.0
0.1
0.2
0.5
1
2
5
10
20
Frequency (Hz)

Figure 8

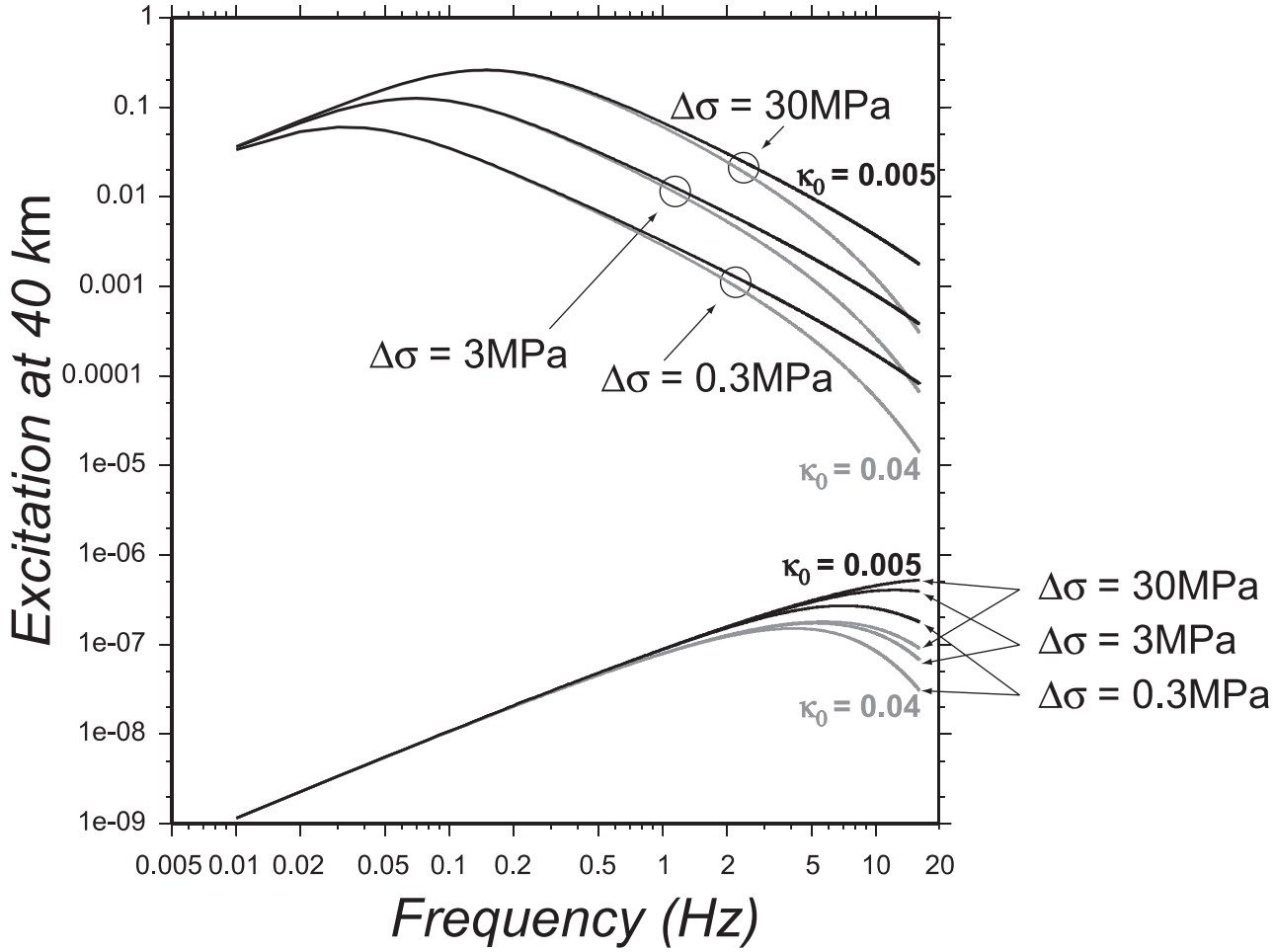
Excitation at 40 km
Frequency (Hz)
1
0.1
0.01
0.001
0.0001
1e-05
1e-06
1e-07
1e-08
1e-09
0.005 0.01 0.02 0.05 0.1 0.2 0.5 1 2 5 10 20
Δσ = 30MPa
κ0 = 0.005
Δσ = 3MPa
Δσ = 0.3MPa
κ0 = 0.04
κ0 = 0.005
κ0 = 0.04
Δσ = 30MPa
Δσ = 3MPa
Δσ = 0.3MPa

Figure 9

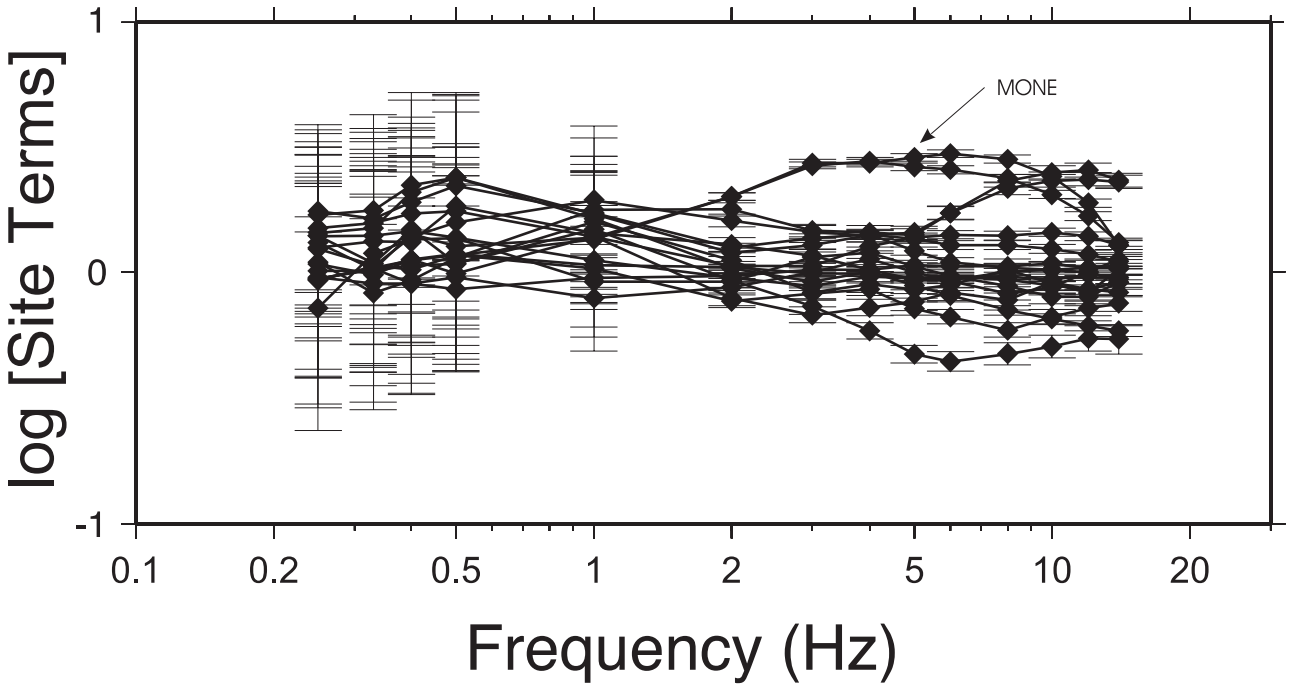

Figure 10

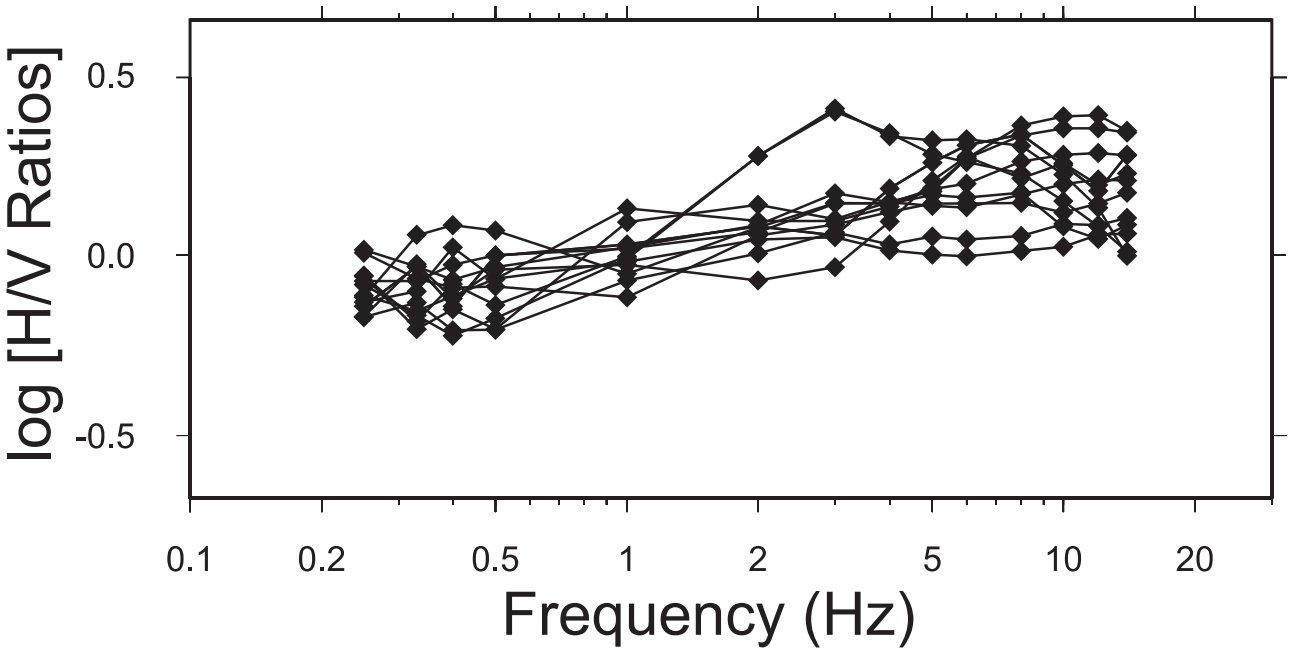

Figure 11

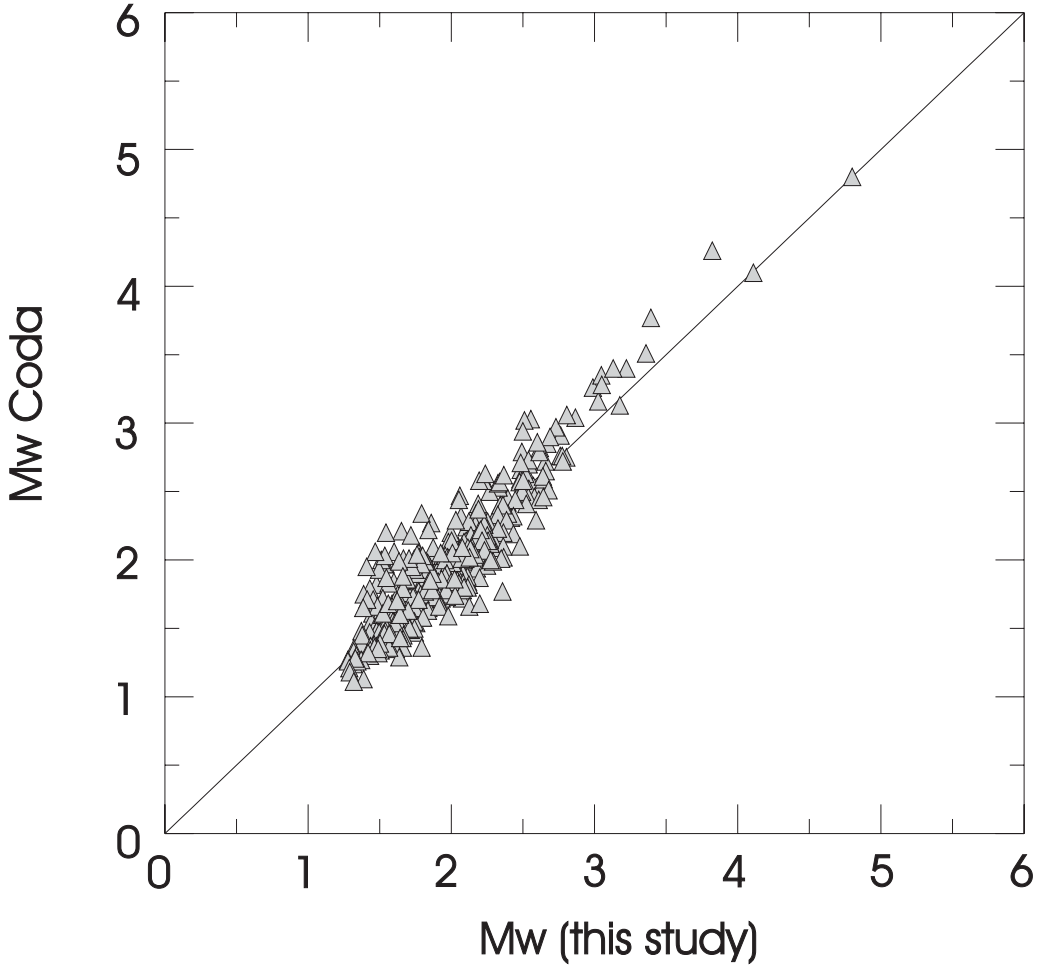

Figure 12

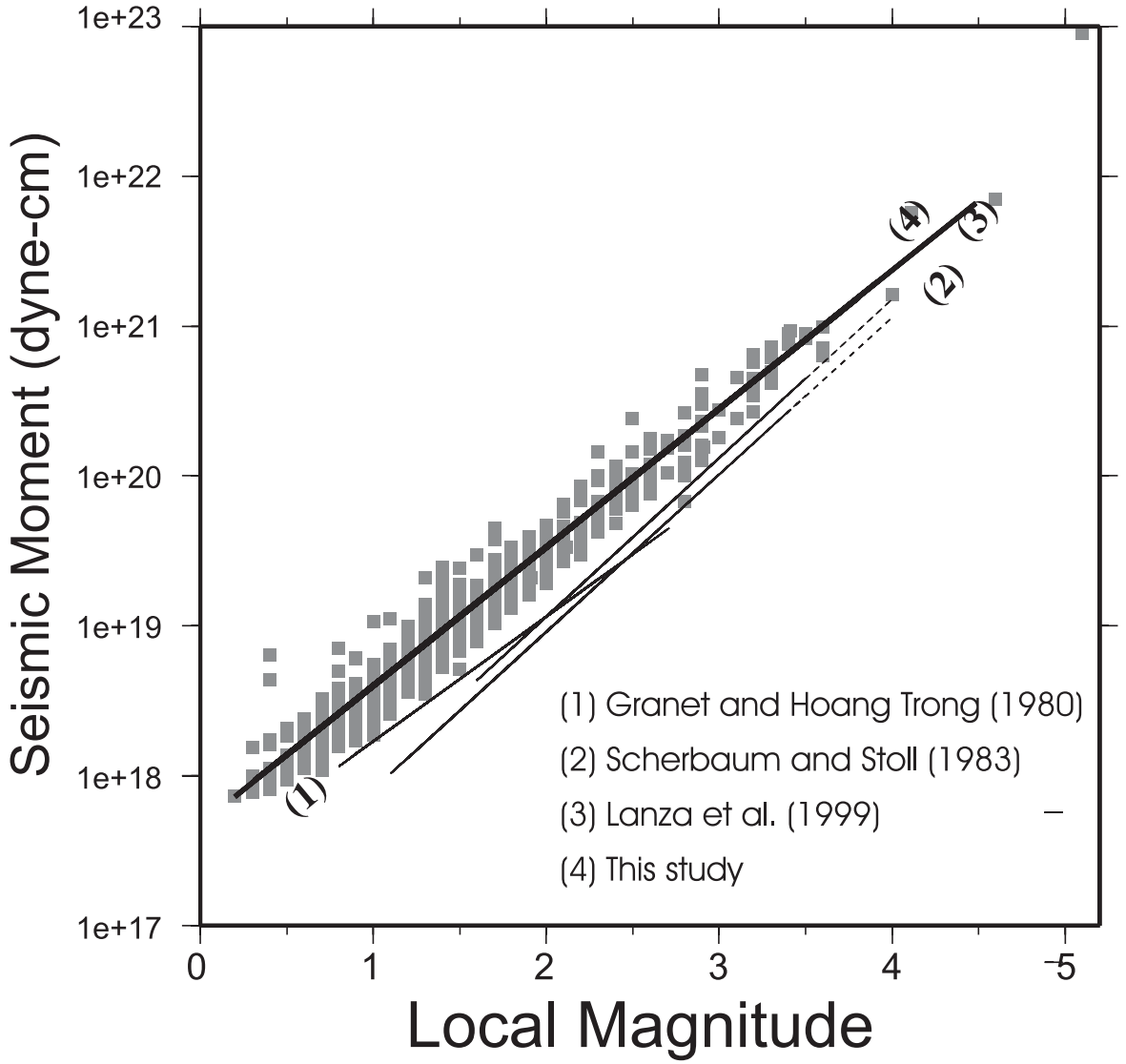
1e+23
1e+22
1e+21
1e+20
1e+19
1e+18
1e+17
Seismic Moment (dyne-cm)
0
1
2
3
4
5
Local Magnitude
(1)
(2)
(3)
(4)
(1) Granet and Hoang Trong (1980)
(2) Scherbaum and Stoll (1983)
(3) Lanza et al. (1999)
(4) This study

Figure 13

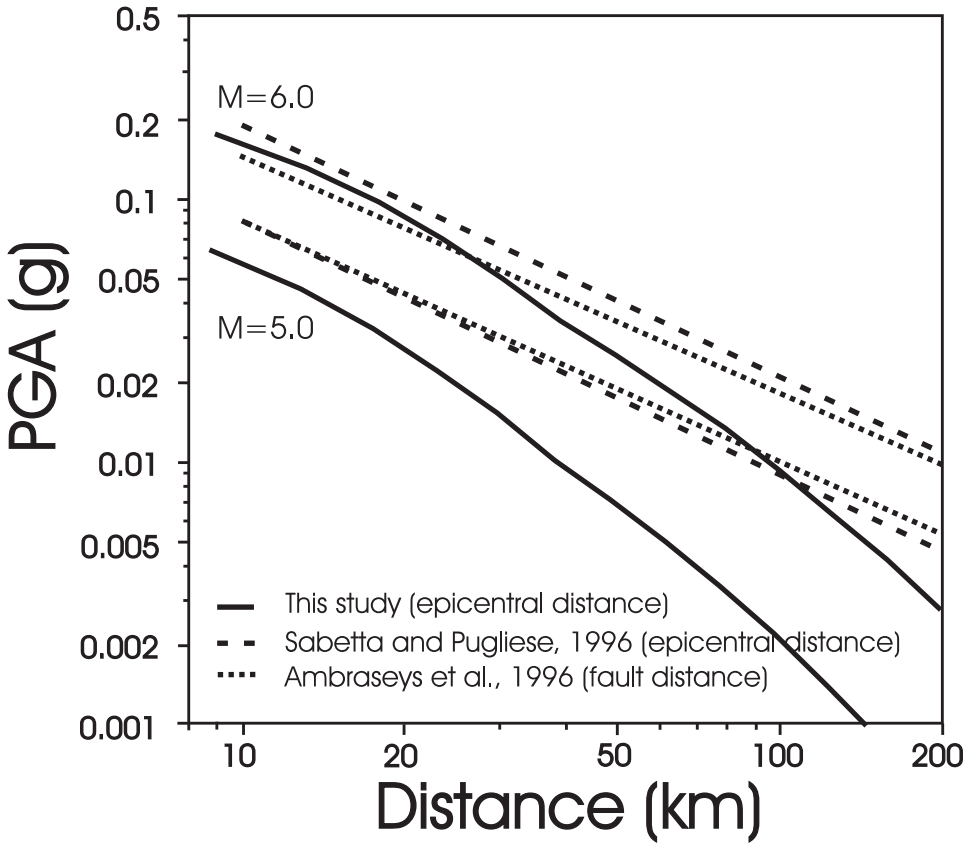
0.5
0.2
0.1
0.05
0.02
0.01
0.005
0.002
0.001
PGA (g)
M=6.0
M=5.0
This study (epicentral distance)
Sabetta and Pugliese, 1996 (epicentral distance)
Ambraseys et al., 1996 (fault distance)
10
20
50
100
200
Distance (km)

Figure 14

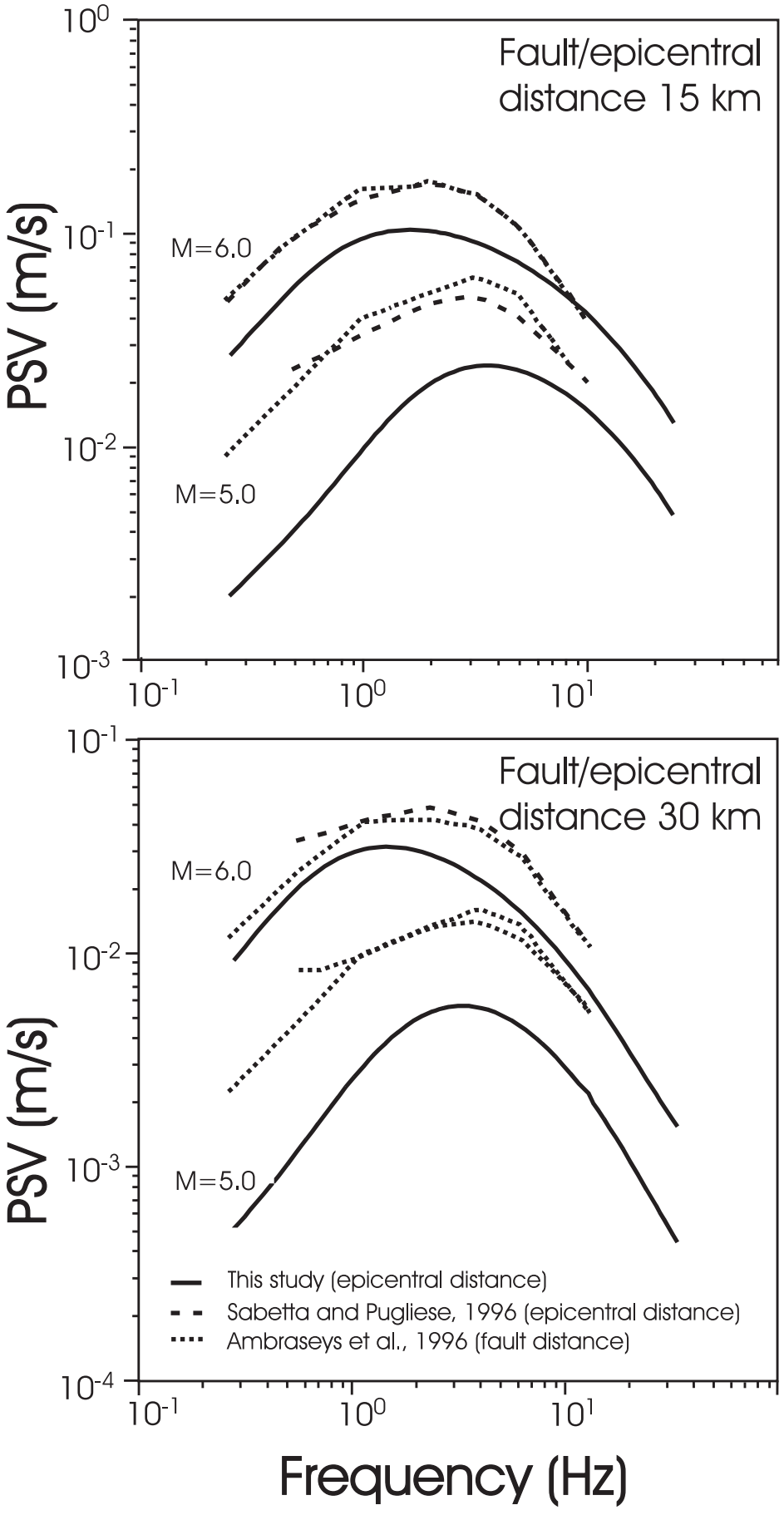
Fault/epicentral
distance 15 km
M=6.0
M=5.0
PSV (m/s)
Fault/epicentral
distance 30 km
M=6.0
M=5.0
PSV (m/s)
This study (epicentral distance)
Sabetta and Pugliese, 1996 (epicentral distance)
Ambraseys et al., 1996 (fault distance)
Frequency (Hz)

Figure 15